Scientia Iranica B (2013) 20 (2), 343–350

Sharif University of Technology
Scientia Iranica
Transactions B: Mechanical Engineering
www.sciencedirect.com

Free turbulent flow emanating from a large plane square nozzle: A theoretical and experimental study

E. Chaparian *, **M.J. Amini**, **A. Sedaghat**

Department of Mechanical Engineering, Isfahan University of Technology, Isfahan 84156, Iran

Received 17 July 2012; revised 16 November 2012; accepted 14 January 2013

KEYWORDS
Turbulence;
Free jet;
Large plane nozzle;
Wind-tunnel.

Abstract Regarding the use of the velocity distribution of turbulent flows of big square plane nozzles, the authors propose the modeling of a turbulent free jet in a wind-tunnel. The free jet mixes with the surrounding fluid, creating turbulence and the jet grows thicker as a result of the exchange of momentum between stagnant air and a portion of the jet. In this study, jets of air ejected from square nozzles of large sizes and flowing into stagnant air are considered. Theoretical solutions based on two different turbulence theories are proposed with coefficients that should be measured experimentally. These coefficients are obtained for a wide range of Reynolds numbers and a correlation is also proposed. In different stations in the axial direction, the velocity distribution appears to have the same shape. This similarity is shown either by theoretical solutions or experimental measurements in this work.

1. Introduction

Experimental observations indicate that in the field of velocity in the axial direction of the jet, the jet flow can be divided into two separate regions: 1. Flow development region, close to the nozzle, in which there is a region of undisturbed velocity surrounded by a mixing layer on top and bottom, as the turbulence penetrates inward the axis of the jet, 2. Fully developed flow region in which the turbulence penetrates into the axis. The region, not influenced by the mixing turbulent layer in the flow development region, is known as the potential core. These regions are shown in Figure 1.

Up to this point experimental research about plane turbulent jets has been focused on plane jets leaving nozzles of small sizes. Tollmien [1] and Görtler [2] solved the equations of motion using different turbulence theorems. Liepmann and Laufer [3] and Wygnanski and Fiedler [4] made experimental observations for thin nozzles. Van der Hegge and Zinjen [5] used a nozzle of size 0.5 × 10 and 1 × 25 cm^2; however, the concerns about the velocity distribution of large plane jets has been increased. The main purpose of this research is to evaluate the velocity profile of a large plane turbulent free jet. In addition, the analytical solutions are validated with present experimental data. The similarity between velocity profiles in different axial direction stations is shown. For experimental observations, the authors propose the modeling of a large plane turbulent jet by wind tunnels with various test section sizes.

2. Governing equations

The equations of motion for the plane turbulent free jet will be developed in this section. The principal equations will be reduced to ordinary differential equations. These equations are obtained by substituting different models of turbulence in equations of motions. The Reynolds equations in the Cartesian system for a steady 2D turbulent flow can be written as [6]:

x-direction:

$$u\frac{\partial u}{\partial x}+\upsilon\frac{\partial u}{\partial y}=-\frac{1}{\rho}\frac{\partial p}{\partial x}+\nu\left(\frac{\partial^2 u}{\partial x^2}+\frac{\partial^2 u}{\partial y^2}\right)-\left(\frac{\partial\overline{u'^2}}{\partial x}+\frac{\partial\overline{u'\upsilon'}}{\partial y}\right)\tag{1}$$

* Correspondence to: University of Tehran, School of Engineering, Department of Mechanical Engineering, P.O. Box 11155-4563, Tehran, Iran. Tel.: +98 913 204 8620; fax: +98 21 8013029.
E-mail address: e.chaparian@ut.ac.ir (E. Chaparian).
Peer review under responsibility of Sharif University of Technology.

Production and hosting by Elsevier

1026-3098
doi:10.1016/j.scient.2013.02.022

Nomenclature

a	Constant
a_1, a_2, a_3	Constants
A_1, A_2, A_3	Constants
bx	Local length of mixing layer (m)
b_1, b_2, b_3	Constants
C	Constant
C_1, C_2	Constants
D_h	Nozzle hydraulic diameter (m)
k	Constant
l	Mixing length (m)
p	Local pressure (N m^{-2})
p_∞	Pressure outside the jet (N m^{-2})
Re_{Dh}	Reynolds number, $U_0 D_h/\nu$
u	Local velocity component in x-direction (m s^{-1})
u'	Local turbulent fluctuation (rms) in the x-direction (m s^{-1})
U_0	Flow velocity in nozzle (m s^{-1})
υ	Local velocity component in y-direction (m s^{-1})
υ'	Local turbulent fluctuation (rms) in the y-direction (m s^{-1})
x	Axial distance measured from the nozzle (m)
y	Distance normal to the axis of the jet (m)
y^*	Value of y where $\upsilon = 0$

Greek letters

β	Constant
$\eta = y/b$	Non-dimensional distance
η^*	Value of η where $\upsilon = 0$
μ	Dynamic viscosity (N s m^{-2})
ν	Kinematic viscosity (m^2 s^{-1})
ν_t	Eddy viscosity (m^2 s^{-1})
$\xi = \sigma y/x$	Non-dimensional distance in Görtler approach
ρ	Fluid density (kg m^{-3})
σ	Distance coefficient
τ_l	Laminar shear stress (N m^{-2})
τ_t	Turbulent shear stress (N m^{-2})
$\phi = y/ax$	Non-dimensional distance in Tollmien approach
ϕ_1	Value of ϕ along the line between mixing layer and potential core
ϕ_2	Value of ϕ along the line between mixing layer and stagnant air
ψ	Stream function.

y-direction:

$$u\frac{\partial \upsilon}{\partial x} + \upsilon\frac{\partial \upsilon}{\partial y} = -\frac{1}{\rho}\frac{\partial p}{\partial y} + \nu\left(\frac{\partial^2 \upsilon}{\partial x^2} + \frac{\partial^2 \upsilon}{\partial y^2}\right) - \left(\frac{\partial \overline{u'\upsilon'}}{\partial x} + \frac{\partial \overline{\upsilon'^2}}{\partial y}\right). \quad (2)$$

And the conservation of mass can be shown by the continuity equation:

$$\frac{\partial u}{\partial x} + \frac{\partial \upsilon}{\partial y} = 0 \quad (3)$$

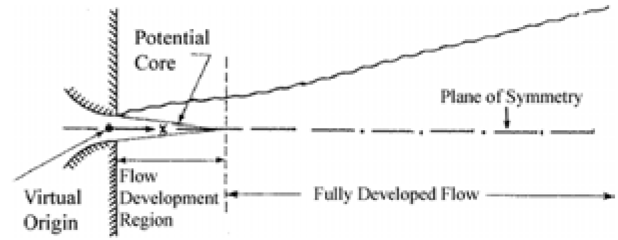

Figure 1: Regions of a turbulent jet.

where the x-axis defines the axial direction of the jet, the y-axis is normal to the x-axis and is in the direction of the height of the nozzle in the coordinate system, u, υ and u', υ' are the turbulent mean and fluctuating velocities in the x- and y-coordinate directions, p is the mean pressure at any point, ν is the kinematic viscosity, and ρ is the density of the fluid.

u is generally larger than υ to a great extent. So the velocity and stress gradients in the y-direction are much larger than those in the x-direction [7]. With these considerations and using an order of magnitude analysis, the equations of motion could be reduced to the form:

$$u\frac{\partial u}{\partial x} + \upsilon\frac{\partial u}{\partial y} = -\frac{1}{\rho}\frac{\partial p}{\partial x} + \nu\frac{\partial^2 u}{\partial y^2} - \frac{\partial \overline{u'\upsilon'}}{\partial y} - \frac{\partial \overline{u'^2}}{\partial x} \quad (4)$$

$$0 = -\frac{1}{\rho}\frac{\partial p}{\partial y} - \frac{\partial \overline{\upsilon'^2}}{\partial y}. \quad (5)$$

Integrating Eq. (5) with respect to y from y to a point located outside the jet yields to $p = p_\infty - \rho\overline{\upsilon'^2}$, where p_∞ is the pressure outside the jet. Substituting in Eq. (4) results in:

$$u\frac{\partial u}{\partial x} + \upsilon\frac{\partial u}{\partial y} = -\frac{1}{\rho}\frac{dp_\infty}{dx} + \nu\frac{\partial^2 u}{\partial y^2} - \frac{\partial \overline{u'\upsilon'}}{\partial y} - \frac{\partial}{\partial x}(\overline{u'^2} - \overline{\upsilon'^2}). \quad (6)$$

The last term in Eq. (6) is smaller than the other terms and could be neglected [8]. Hence:

$$u\frac{\partial u}{\partial x} + \upsilon\frac{\partial u}{\partial y} = -\frac{1}{\rho}\frac{dp_\infty}{dx} + \nu\frac{\partial^2 u}{\partial y^2} - \frac{\partial \overline{u'\upsilon'}}{\partial y}. \quad (7)$$

In Eq. (7) the last two terms can be written as below to show how the shear stresses influence the equations of motion:

$$\frac{1}{\rho}\frac{\partial}{\partial y}\left(\mu\frac{\partial u}{\partial y}\right) + \frac{1}{\rho}\frac{\partial}{\partial y}(-\rho\overline{u'\upsilon'}) = \frac{1}{\rho}\frac{\partial}{\partial y}(\tau_l + \tau_t) \quad (8)$$

where τ_l and τ_t are the laminar and turbulent shear stresses, respectively, and μ is the dynamic viscosity. In free turbulent flow because of the absence of solid boundaries, τ_t is much larger than τ_l [6]. So, it is reasonable to neglect τ_l and rewrite Eq. (8) as:

$$u\frac{\partial u}{\partial x} + \upsilon\frac{\partial u}{\partial y} = -\frac{1}{\rho}\frac{dp_\infty}{dx} + \frac{1}{\rho}\frac{\partial \tau_t}{\partial y}. \quad (9)$$

Furthermore, because the plane turbulent free jet with a zero pressure gradient in the axial direction is considered it can be assumed that $dp_\infty/dx = 0$. Thus Eq. (9) is reduced to:

$$u\frac{\partial u}{\partial x} + \upsilon\frac{\partial u}{\partial y} = \frac{1}{\rho}\frac{\partial \tau_t}{\partial y}. \quad (10)$$

Eqs. (3) and (10) are the final equations of motion contemplated in this paper for the plane turbulent free jet with a zero pressure gradient in the axial direction.

3. Theoretical solutions

There are three unknown parameters, u, υ, and τ_t in Eqs. (3) and (10). The authors utilize a turbulence model to close this set of equations. In this paper two models are considered; Prandtl's mixing length formula and Prandtl's equation for turbulent shear stress. The potential core is a region of undiminished mean velocity, U_0. The intense shear at the surface of velocity discontinuity induces turbulence and the stagnant fluid is accelerated since a portion of the jet loses some momentum. The thickness of the fluid layer affected by this exchange of momentum which is known as the mixing layer could be denoted as b at any x-station. The similarity of velocity profiles makes it reasonable to assume that $u/U_0 = \hat{f}(y/b) = \hat{f}(\eta)$ and $\tau_t/\rho U_0^2 = g(\eta)$. Hence:

$$\frac{\partial u}{\partial x} = U_0\left[\hat{f}'\left(\frac{-\eta}{b}\right)b'\right] \tag{11}$$

where $\hat{f}' = \partial\hat{f}/\partial\eta$ and $b' = \partial b/\partial x$.

$$\upsilon = \int_{y^*}^{y}\frac{\partial\upsilon}{\partial y}dy \tag{12}$$

where y^* is the value of y where $\upsilon = 0$.

$$\upsilon = -\int_{y^*}^{y}\frac{\partial u}{\partial x}dy. \tag{13}$$

Substituting Eq. (11) into Eq. (13) results in:

$$\upsilon = U_0 b'\left[F_1(\eta) - F_1(\eta^*)\right] \tag{14}$$

where $\int \eta\hat{f}'\,d\eta = F_1(\eta)$ and $\eta^* = y^*/b$.

Substituting these expressions in the momentum equation results in:

$$g' = -b'(\eta\hat{f}\,\hat{f}' - \hat{f}'\,F_1) - b'F_1(\eta^*)\hat{f}'. \tag{15}$$

Since g' is only a function of η, b', and $F_1(\eta^*)$ should be independent of x. Hence:

$$b = Cx. \tag{16}$$

3.1. Tollmien approach

For the needed extra equation the Prandtl mixing length formula is considered [9]:

$$\tau_t = \rho l^2(\partial u/\partial y)^2 \tag{17}$$

where l is the mixing length.

$$l = \beta b = \beta Cx. \tag{18}$$

F can be defined such that:

$$u/U_0 = \hat{f}(y/b) = F'(\phi) \tag{19}$$

where $\phi = y/ax$.

The so-called stream function ψ can be defined such that $u \equiv \partial\psi/\partial y$, $\upsilon \equiv -\partial\psi/\partial x$ [6]. By integrating:

$$\psi = U_0 axF. \tag{20}$$

Thus, υ can be determined:

$$\upsilon = aU_0(\phi F' - F). \tag{21}$$

Further if the value of a is chosen as $a^3 = 2\beta^2C^2$ then:

$$\frac{1}{\rho}\frac{\partial\tau_t}{\partial y} = \frac{U_0^2}{x}(F''F'''). \tag{22}$$

Substituting the above expressions into a momentum equation:

$$-\frac{U_0^2}{x}\phi F'F'' + \frac{U_0^2}{x}F''(\phi F' - F) = \frac{U_0^2}{x}(F''F''')$$

$$\text{Or: } F''(F + F''') = 0. \tag{23}$$

The trivial solution of Eq. (23) is $F'' = 0$, indicating that a uniform distribution for u can be concluded. Another solution to Eq. (23) can be obtained by solving the linear differential equation $F + F''' = 0$. For the boundary conditions it can be assumed that along the line between the mixing layer and potential core $u = U_0$ and $\partial u/\partial y = 0$. In addition, along the line between the mixing layer and the stagnant air out of the jet $u = 0$ [1] and $\partial u/\partial y = 0$. So $F'(\phi_1) = 1$, $F''(\phi_1) = 0$, $F'(\phi_2) = 0$, and $F''(\phi_2) = 0$ where ϕ_1 is the magnitude of ϕ when we move through the line between the mixing layer and the potential core. ϕ_2 is the magnitude of ϕ in the plane between the mixing layer and stagnant air. It can be assumed that along the upper line of the mixing layer $\upsilon = 0$ [1]. So the general solution for Eq. (23) is:

$$F(\phi) = A_1e^{-\phi} + A_2e^{\frac{\phi}{2}}\cos\left(\frac{\sqrt{3}}{2}\phi\right) + A_3e^{\frac{\phi}{2}}\sin\left(\frac{\sqrt{3}}{2}\phi\right). \tag{24}$$

Using boundary conditions, $\phi_1 = 0.981$, $\phi_2 = -2.04$, $A_1 = -0.0176$, $A_2 = 0.134$, and $A_3 = 0.688$.

3.2. Görtler approach

Considering Prandtl's equation for turbulent shear stress [9]:

$$\tau_t = \rho\nu_t\frac{\partial u}{\partial y} \tag{25}$$

where ν_t is the eddy viscosity. Görtler [2] assumed that $\nu_t = kU_0b$ where k is a constant. Using Eq. (16), it can be written as $\tau_t = \rho kU_0Cx(\partial u/\partial y)$. Considering Eq. (20), the stream function can be assumed as $\psi = UxF(\xi)$, where $U = U_0/2$ and $\xi = \sigma y/x$. σ is a constant which will be discussed later. Thus $u = U\sigma F'$ and $\upsilon = U(\xi F' - F)$ where $F' = \partial F/\partial\xi$. So, the momentum equation can be rewritten:

$$-\frac{\sigma^2U^2}{x}\xi F'F'' + \frac{\sigma^2U^2}{x}F''(\xi F' - F) = 2kC\sigma^3\frac{U^2}{x}F'''$$

$$\text{or: } F''' + \frac{1}{2kC\sigma}FF'' = 0. \tag{26}$$

If $\sigma = 1/2\sqrt{kC}$ then Eq. (26) can be written as:

$$F''' + 2\sigma FF'' = 0. \tag{27}$$

To solve Eq. (27), H can be defined as $H'(\xi) = F''(\xi)$. Also Görtler [2] assumed a series of the form:

$$\sigma F = \xi + F_1(\xi) + F_2(\xi) + \cdots. \tag{28}$$

Substituting into Eq. (27), in the first approximation, it can be written as $H''(\xi) + 2\xi H'(\xi) = 0$. Hence:

$$F'(\xi) = C_1\int_0^{\xi}\exp(-z^2)dz + C_2. \tag{29}$$

Boundary conditions are $F'(-\infty) = 0$ and $F'(\infty) = 2/\sigma$.

So C_1 and C_2 can be calculated as $2/(\sigma\sqrt{\pi})$ and $1/\sigma$, respectively. Hence:

$$\frac{u}{U_0} = \frac{1}{2}(1 + erf(\xi)). \tag{30}$$

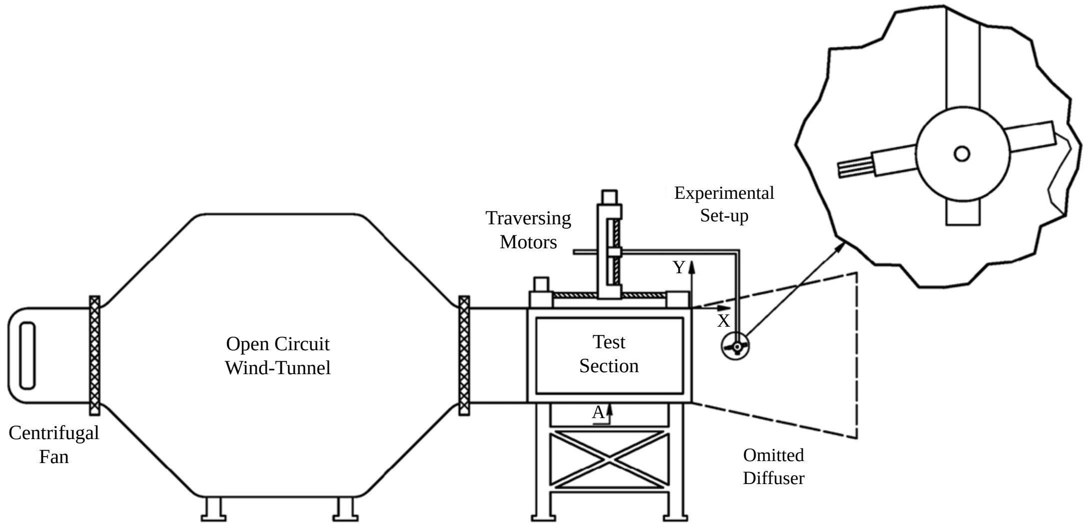

Figure 2: Experimental setup.

4. Experimental setup

The experiments were conducted out of the square test section of the subsonic blower wind-tunnels of an open return type (wind speeds up to 30 m s^{-1}). The contraction section of the tunnel first leads to a straight section which is then followed by the test section and diffuser. It is practical to model the plane turbulent free jet by omitting the diffuser and letting the wind be mixed with stagnant air after leaving the test section. The measurements were conducted in a wide range of free-stream velocities with turbulence intensity levels of less than 0.2% of the free-stream velocity. The flow uniformity in the spanwise direction was confirmed by a series of measurements conducted in the spanwise extent at Section A. A schematic diagram of the wind-tunnel and experimental setup is shown in Figure 2.

The experimental results are measured using a constant-temperature hot-wire anemometry system [10–13] pitched to a probe coming out of the test sections. Tests were carried out with two hot-wire probes. The calibration of the hot-wires was carried out in the test section. Mean velocity, velocity fluctuations, and shear stress investigated for the turbulent flow of air covering a Reynolds number range from 6×10^4 to 1.8×10^6. The probe is traversed across the height of the tunnels and through x-direction in the symmetry plane of nozzles in the y-direction. At each measuring station in the axial direction, 11 V readings were taken, each 10 times, to reduce experimental uncertainty. Measurement uncertainty is calculated using the Jørgensen's method [14]. This method calculated the total uncertainty from individual errors in the calibration, data conversion, and experimental conditions. The measurement uncertainty for hot-wire probes was estimated to be 3.1% for the mean and turbulence fluctuations, and 6.2% for turbulence shear stress.

5. Results and discussion

The theories applied in Tollmien and Görtler approaches can be compared with experimental results. The applicability of the turbulence models to the flow under investigation is thoroughly verified by comparison of the turbulence statistics in the present study.

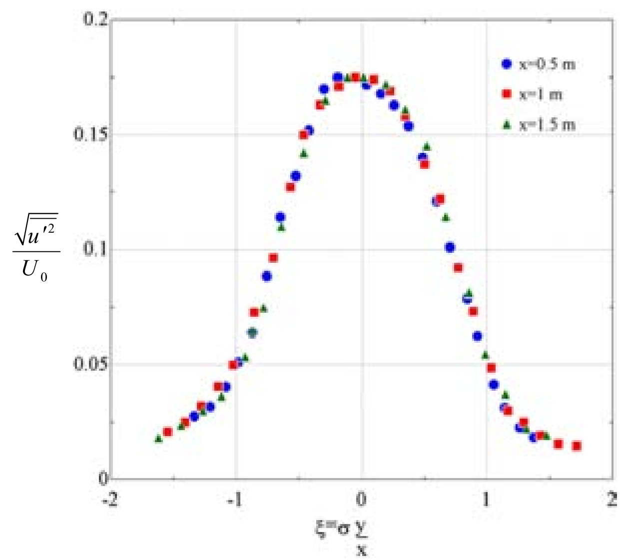

Figure 3: First component of velocity fluctuations, $\sigma = 9$, $Re_{Dh} = 10^6$.

5.1. Turbulence statistics

The turbulence fluctuations are measured in the mixing layer of the flow development region. Figures 3 and 4 show the distribution of two velocity fluctuations in a dimensionless manner. The mean velocity in the nozzle and potential core is used to non-dimensionalize the fluctuations. Also it should be noted that y is measured from the plane where $u = 0.5U_0$. The notes about σ are discussed in detail in Section 5.2. Figures 3 and 4 show that in the origins near the $y = 0$ plane the turbulence intensity is larger than in any other origins. The shear stress measurements are shown in Figure 5. It is seen that the experimental results are in satisfactory agreement with the curves calculated by the developed theories.

5.2. Comparison of mean velocity

Liepmann and Laufer [3] in their experimental observations for thin nozzles with big aspect ratios found that the model is

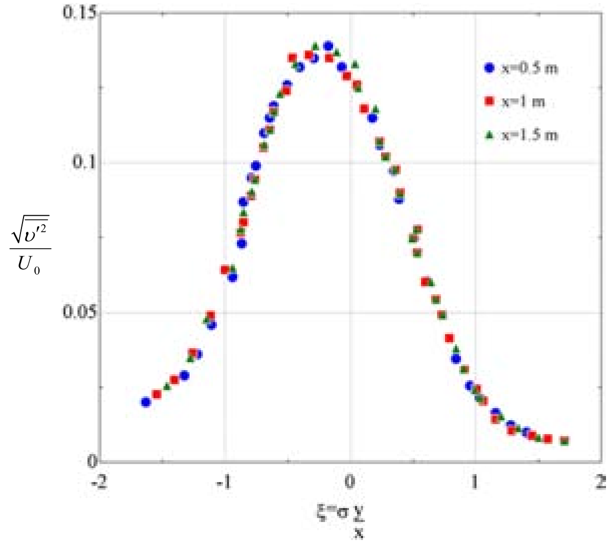

Figure 4: Second component of velocity fluctuations, $\sigma = 9$, $Re_{Dh} = 10^6$.

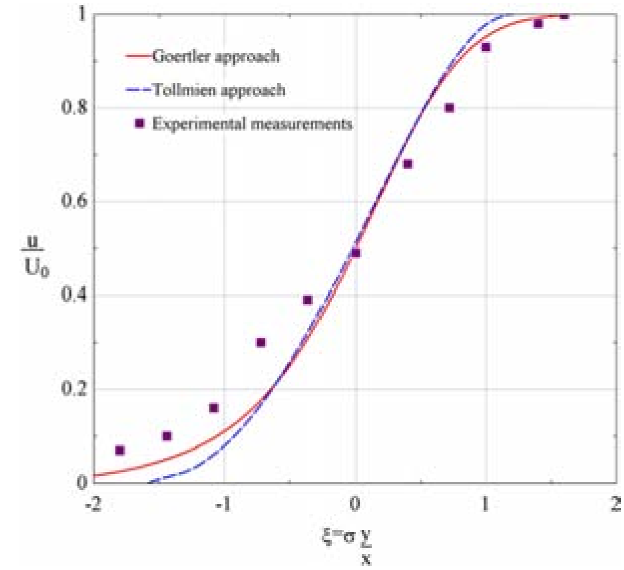

Figure 6: Velocity profile at $x = 1$ m, $\sigma = 11$, $Re_{Dh} = 10^6$.

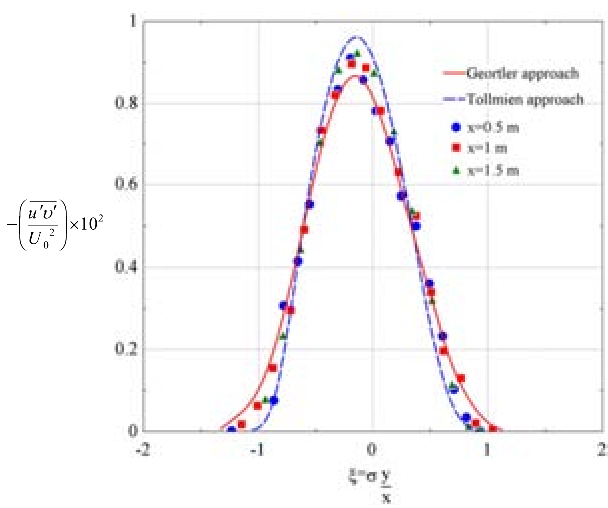

Figure 5: Shear stress, $\sigma = 9$, $Re_{Dh} = 10^6$.

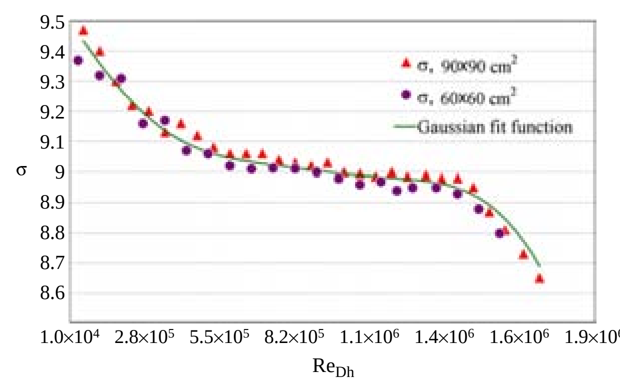

Figure 7: σ versus Re_{Dh}.

correlated with Tollmien and Görtler solutions when a value of $\sigma = 11$ is selected. Testing various speeds in wind-tunnels at multiple stations, the authors plot u/U_0 obtained by the theoretical solutions and experimental modeling results versus ξ for the chosen Reynolds numbers and stations. The transverse distance, y, is measured from the point at which $u = 0.5U_0$ in all figures.

As seen in Figure 6, the similarity of velocity profiles of different approaches is explicitly apparent but for $\sigma = 11$, the analytical solutions do not appropriately agree with experimental measurements. As mentioned σ was acquired through experimental investigations for thin nozzles. In the present work, the goal is to obtain the velocity distribution for square nozzles of a large size. Experimental measurement analyses show that the magnitude of σ is not constant. σ is independent of x (distance from the nozzle) while the size of the nozzle and U_0 have a great influence on the magnitude of σ. By defining the Reynolds number based on the flow in the test section, U_0D_h/ν, the two important factors can be considered simultaneously. Measuring σ for the Reynolds number range considered in the wind-tunnel modeling, the authors plot Figure 7 to show the result.

The relation between σ and the Reynolds number can be seen by Eq. (31) which is determined by the Gaussian fit function.

$$\sigma(Re_{Dh}) = \sum_{i=1}^{3} a_i \exp\left(-\left(\frac{Re_{Dh} - b_i}{c_i}\right)^2\right) \qquad (31)$$

$$6 \times 10^4 < Re_{Dh} < 1.8 \times 10^6$$

where:

$a_1 = 10.31$, $b_1 = -8.891 \times 10^5$,
$c_1 = 2.602 \times 10^6$, $a_2 = 5.232$, $b_2 = 1.97 \times 10^6$,
$c_2 = 1.169 \times 10^6$, $a_3 = 0.3348$,
$b_3 = 7.901 \times 10^5$, $c_3 = 5.22 \times 10^5$.

To show this functionality, the authors plot Figures 8–13 which show u/U_0 versus ξ (calculated by σ determined using Eq. (31)) with very small deviations between different approaches for 3 sample Reynolds numbers. As is obvious, the Tollmien approach near the axis of the jet is superior but in the outer region the Görtler approach predicts the velocity

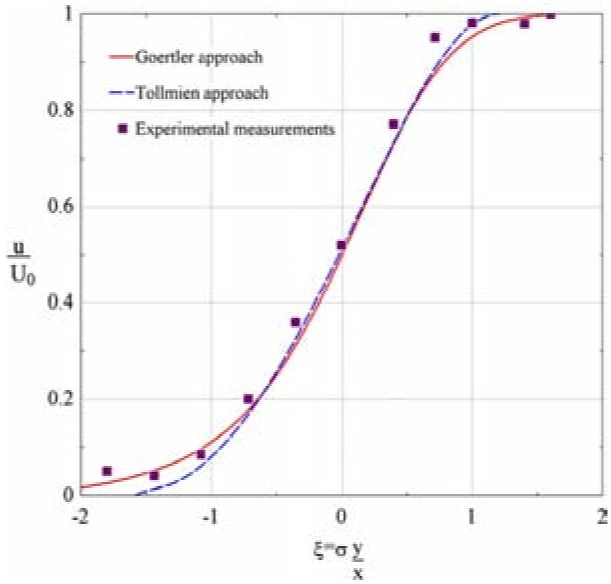

Figure 8: Velocity profile at $x = 1$ m, $\sigma = 9.12$, $Re_{Dh} = 4 \times 10^5$, test section 60×60 cm^2.

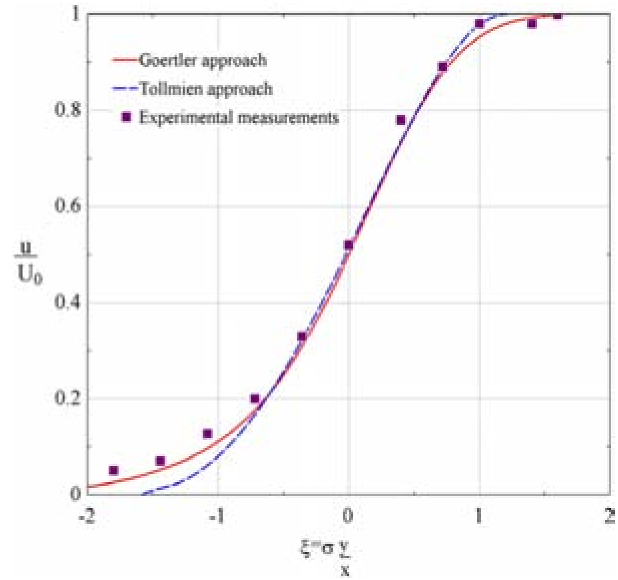

Figure 10: Velocity profile at $x = 1$ m, $\sigma = 9$, $Re_{Dh} = 10^6$, test section 60×60 cm^2.

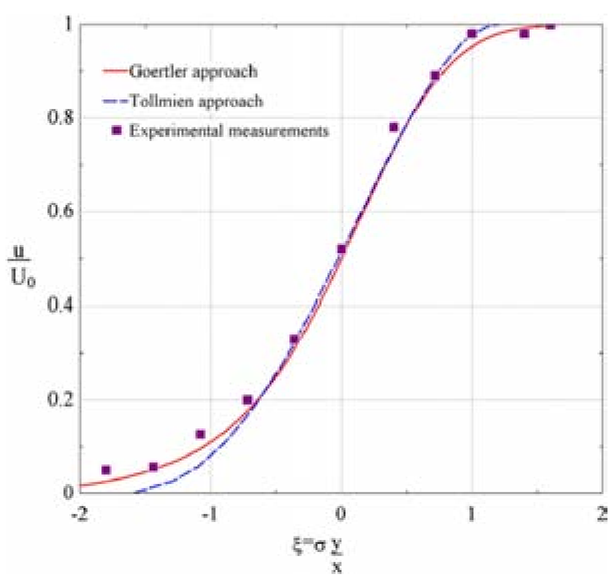

Figure 9: Velocity profile at $x = 1$ m, $\sigma = 9.12$, $Re_{Dh} = 4 \times 10^5$, test section 90×90 cm^2.

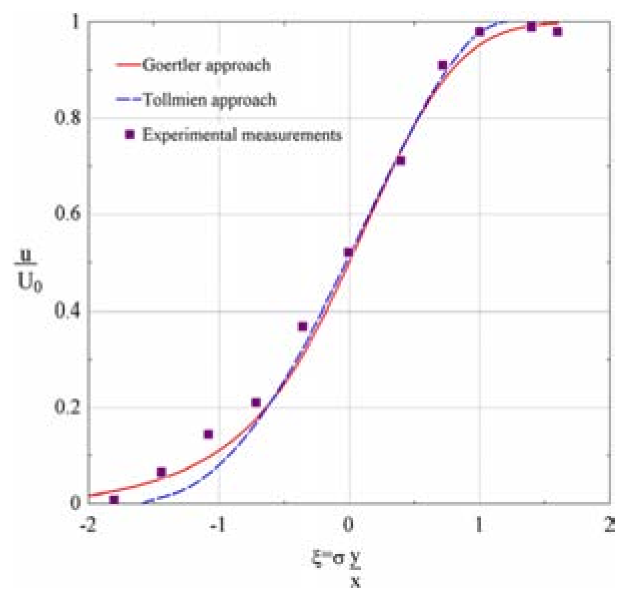

Figure 11: Velocity profile at $x = 1$ m, $\sigma = 9$, $Re_{Dh} = 10^6$, test section 90×90 cm^2.

distribution with great precision. As used before, for different stations in x-direction by using non-dimensional parameters, all velocity distributions have the same shape and are similar, as concluded from Figures 14 and 15 which show the velocity profile versus ξ at different stations for two nozzle sizes.

6. Conclusion

A methodology has been presented to accurately model the plane turbulent free nozzle flow conditions out of the test sections of open-circuit wind-tunnels. The methodology is based on determining the relationship between the velocity profiles in different stations and non-dimensional distances. The similarity was revealed by experimental measurements which have significant correlation with theoretical solutions. The mentioned correlation was not satisfactory by the constants measured for thin nozzles but by ones obtained for big square nozzles with unity aspect ratios, tested as experimental models in this research, they are extremely good.

Acknowledgments

The authors gratefully acknowledge Dr. M. Talebi for his assistance in the wind-tunnel measurements. Also, the authors would like to express special thanks to Professors Shirani, Sadeghy, and Mina Oghanian for their invaluable guidance.

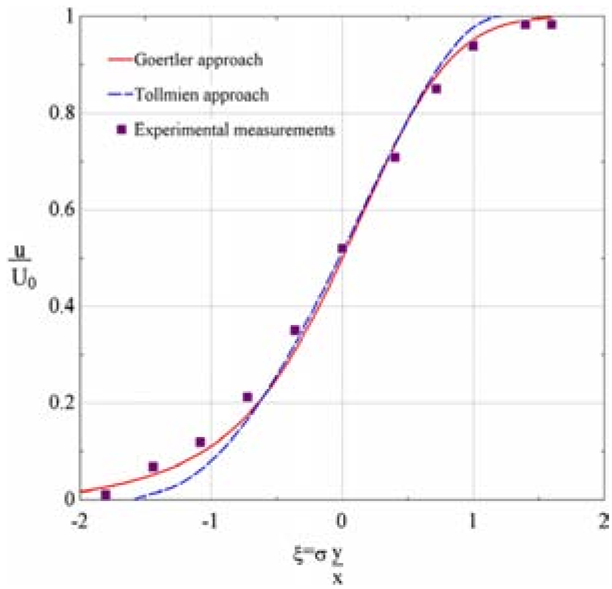

Figure 12: Velocity profile at $x = 1$ m, $\sigma = 8.89$, $Re_{Dh} = 1.6 \times 10^6$, test section 60 × 60 cm^2.

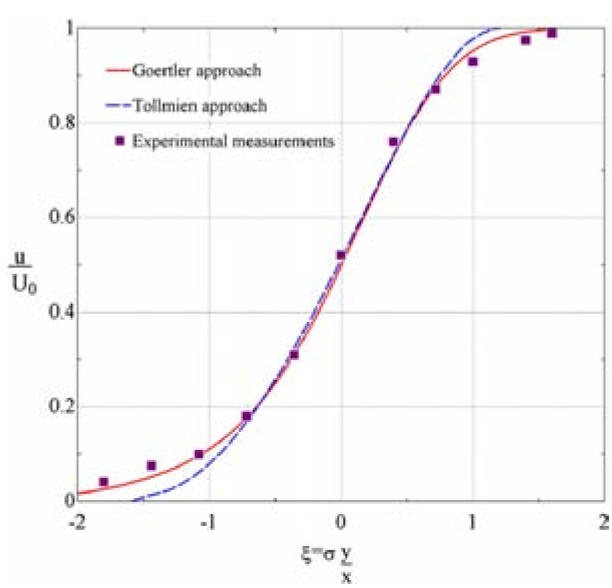

Figure 13: Velocity profile at $x = 1$ m, $\sigma = 8.89$, $Re_{Dh} = 1.6 \times 10^6$, test section 90 × 90 cm^2.

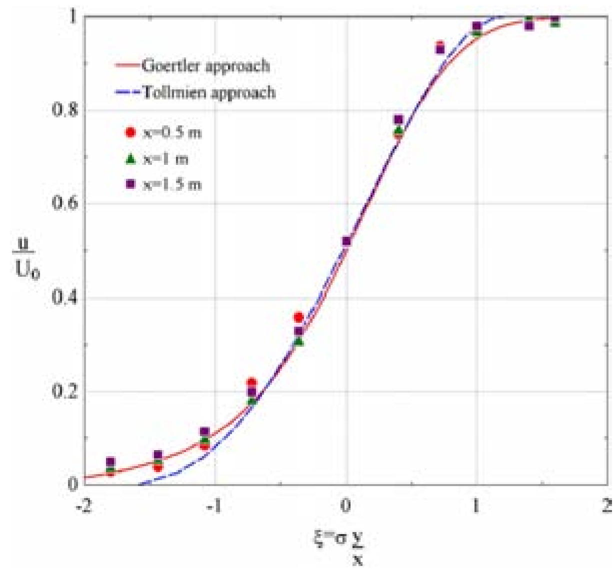

Figure 14: Similarity of velocity profiles at various stations, test section 60 × 60 cm^2.

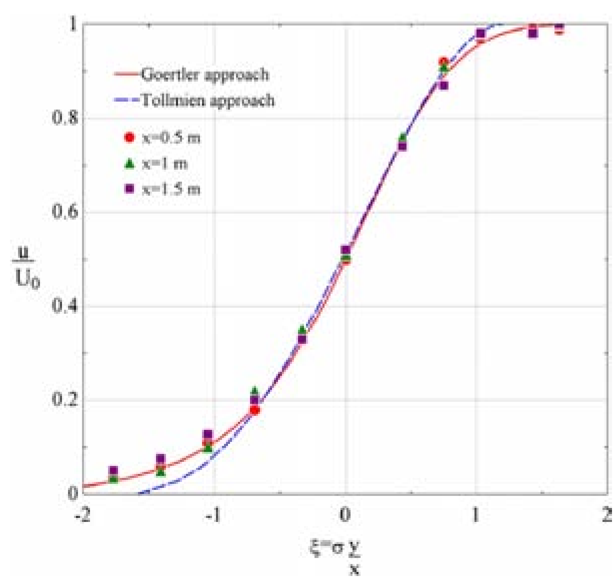

Figure 15: Similarity of velocity profiles at various stations, test section 90 × 90 cm^2.

References

[1] Tollmien, W. "Berechnung turbulenter Ausbreitungsvorgänge", *ZAMM*, 6(6), pp. 468–478 (1926).
[2] Görtler, H. "Berechnung von Aufgaben der freien Turbulenz auf Grund eines neuen Näherungsansatzes", *ZAMM*, 22(5), pp. 244–254 (1942).
[3] Liepmann, H.W. and Laufer, J. "Investigation of free turbulent mixing", NACA TN No. 1257, Washington (1947).
[4] Wygnanski, L. and Fiedler, H. "The two-dimensional mixing region", *Cambridge J. Fluid Mech.*, 41(2), pp. 327–361 (1970).
[5] Van der Hegge, B.G. and Zinjen, "Measurements of the velocity distribution in a plane turbulent jet of air", *Appl. Sci. Res.*, 7(4), pp. 256–276 (1958).
[6] Biswas, G. and Eswaran, V., *Turbulent Flows: Fundamentals, Experiments and Modeling*, 1st Edn., CRC Press (2002).
[7] Cebeci, T. and Cousteix, J., *Modeling and Computation of Boundary-Layer Flows: Laminar, Turbulent and Transitional Boundary Layers in Incompressible Flows*, 2nd Edn., Springer, New York (2005).
[8] Pope, S.B., *Turbulent Flows*, Cambridge University Press (2000).
[9] Rodi, W. and Spalding, D.B. "A two-parameter model of turbulence, and its application to free jets", *Heat Mass Transfer*, 3(2), pp. 85–95 (1970).
[10] Haasl, S., Stemme, G., Gianchandani, Y., Tabata, O. and Zappe, H., *Comprehensive Microsystems, Flow Sensors*, Elsevier pp. 209–272 (2007).
[11] Heskestad, G. "Hot-wire measurements in a plane turbulent jet", *ASME J. Appl. Mech.*, 32, pp. 721–734 (1965).
[12] Thompson, W.P., *Methods of Experimental Physics: Fluid Dynamics, 18*, R. Emrich, Ed., pp. 457–463, Academic Press, New York Part B (1981).
[13] Bruun, H.H., *Hot-Wire Anemometry: Principles and Signal Analysis*, Oxford University Press Inc., New York (1995).
[14] Jørgensen, F.E. "How to measure turbulence with hot-wire anemometers—a practical guide", *DANTEC Dynamics*, Denmark (2005).

Emad Chaparian obtained his B.S. degree from Isfahan University of Technology, Isfahan, Iran, in 2011, and is currently an M.S. degree student in the Mechanical Engineering Department at the University of Tehran, Iran. His main research interests include: hydrodynamic instability and turbulence, and non-Newtonian fluid mechanics.

Mohammad Javad Amini received his B.S. and M.S. degrees in Thermo-Fluid Sciences from the Mechanical Engineering Department at Isfahan University of Technology, Iran, in 2007 and 2011, respectively, and is currently working on the experimental study and mathematical modeling of various cases in fluid mechanics and heat transfer. His major research interests include: experimental investigation of turbulent flows.

Ahmad Sedaghat obtained his Ph.D. degree in Aerospace Engineering from the University of Manchester, UK, in 1997, and is currently Assistant Professor at Isfahan University of Technology, Iran. He has also undertaken various postdoctoral research fellowships at various institutions abroad. His main research interests are in the field of renewable energy and the aerodynamic/aeroelasticity of wind turbines.